COBEM 2023 27TH INTERNATIONAL CONGRESS OF MECHANICAL ENGENEERING

ABCM Brazilian Society of Mechanical Sciences and Engineering
27th ABCM International Congress of Mechanical Engineering
December 04-08, 2023, Florianópolis-SC, Brazil

COB-2023-0055
DEVELOPMENT, IMPLEMENTATION AND VERIFICATION OF AN MHD COMPRESSIBLE SOLVER IN OPENFOAM

Gabriel Fernandes Marconcini Roberto
Juan Pablo de Lima Costa Salazar
Engenharia Aeroespacial, Universidade Federal de Santa Catarina - UFSC
Rua Dona Francisca, 8300 – Bloco U Zona Industrial Norte, Joinville – SC – Brasil - CEP: 89.219-600
gabriel.marconcini@grad.ufsc.br, juan.salazar@ufsc.br

Abstract. *Advancements over the last decades in CFD have made the simulation of increasingly complex flows a reality. Among these are MHD flows, where the electromagnetic effects are a prominent feature of the flow field, leading to a wide range of relevant and interesting phenomena. In this work, we implement a solver for compressible MHD flows within the framework of the open source CFD code OpenFOAM, named mhdCentralFoam. The mhdCentralFoam solver uses a density-based method with semi-discrete central-upwind schemes and a hyperbolic-parabolic advection equation for treatment of the magnetic field divergence free condition. The verification of the solver was performed by comparing the hydrodynamics and MHD solutions to the results available in the literature using two test cases: Hartmann flow and the Brio-Wu shock tube. The mhdCentralFoam solver was able to capture the physical phenomena involved and produced accurate results for the solution of compressible MHD flows.*

Keywords: *magnetohydrodynamics, computational fluid dynamics, compressible, OpenFOAM*

1. INTRODUCTION

Advancements in computational fluid dynamics (CFD) have led to the development of powerful tools capable of simulating increasingly complex flows over a wide variety of conditions, including magnetohydrodynamics (MHD). MHD is a field of study that explores the intricate interaction between magnetic fields and moving conducting fluids, such as liquid metals, strong electrolytes, and plasma (Davidson, 2001).

One notable CFD tool that has emerged over the past two decades is the library Open Source Field Operation and Manipulation (OpenFOAM), which employs the finite volume method (FVM). OpenFOAM is based on object-oriented programming in C++ and provides a syntactic model for equation representation and facilitates scalar-vector-tensor operations (Chen *et al.*, 2014). While OpenFOAM offers the *mhdFoam* application for solving MHD flows, it is currently limited to incompressible laminar flows and does not encompass compressible problems. These compressible scenarios include magnetoplasmadynamic thrusters, geophysical and astrophysical models, and magnetic nozzles, which exhibit discontinuities and other compressibility effects (Tang and Wang, 2015).

To address this limitation, this work presents the implementation and verification of an application within the OpenFOAM framework that can solve compressible MHD flows, covering the subsonic to supersonic regime. For this purpose, a solver based on the method described by Mayigué and Groll (2016) was implemented, utilizing a density-based approach with semi-discrete central-upwind schemes and a hyperbolic-parabolic advection equation to ensure the divergence-free condition of the magnetic field.

The work is structured as follows. Section 2 presents the MHD governing equations, the hypotheses assumed for ideal and non-ideal MHD problems and a discussion about the divergence free condition and the cleaning method used. Section 3 follows with the algorithmic description of *mhdCentralFoam*. To verify the solution produced by the new solver, two cases with analytical or very well documented solutions are compared in Section 4.

2. GOVERNING EQUATIONS

2.1 Magnetohydrodynamics equations

The mathematical formulation of MHD flows is derived from the coupling of the conservation laws of hydrodynamics with Maxwell's equations of electromagnetism. A highly conducting fluid is typically assumed, meaning that the relaxation time for charge redistribution is much shorter than the transit time of electromagnetic waves, i.e., a non-relativistic plasma regime (Moreau, 1990). This assumption allows the displacement current to be neglected and the conservation

laws for MHD flows are expressed as:

$$\frac{\partial \rho}{\partial t} + \nabla \cdot (\rho \mathbf{U}) = 0 \ , \tag{1}$$

$$\frac{\partial \rho \mathbf{U}}{\partial t} + \nabla \cdot (\rho \mathbf{U}\mathbf{U}) = -\nabla P_G + \nabla \cdot \tau_{\mathbf{visc}} + \frac{1}{\mu_0} \nabla \cdot (\mathbf{B}\mathbf{B}) \ , \tag{2}$$

$$\begin{aligned} \frac{\partial \rho E}{\partial t} + \nabla \cdot (\rho E \mathbf{U}) = &- \nabla \cdot (P_G \mathbf{U}) + \nabla \cdot (\tau_{\mathbf{visc}} \cdot \mathbf{U}) + \frac{1}{\mu_0} \nabla \cdot [\mathbf{B} (\mathbf{B} \cdot \mathbf{U})] \\ &+ \nabla^2 \left(\frac{B^2}{2 {\mu_0}^2 \sigma} \right) - \frac{1}{{\mu_0}^2 \sigma} [\nabla \cdot (\nabla (\mathbf{B}\mathbf{B}))] \ , \end{aligned} \tag{3}$$

$$\frac{\partial \mathbf{B}}{\partial t} + \nabla \cdot (\mathbf{U}\mathbf{B} - \mathbf{B}\mathbf{U}) = \frac{1}{\mu_0 \sigma} \nabla^2 \mathbf{B} \ , \tag{4}$$

$$\nabla \cdot \mathbf{B} = 0 \ , \tag{5}$$

where ρ is the fluid density, $\mathbf{U}$ is the velocity vector, $\mathbf{B}$ is the magnetic field vector, $\boldsymbol{\tau}_{\text{visc}}$ is the viscous stress tensor, μ_0 is the magnetic permeability, σ is the electric conductivity, P_G is the overall pressure and E is the total specific energy, given as,

$$E = e + \frac{1}{2} U^2 + \frac{1}{2} \frac{B^2}{\mu_0 \rho} \ , \tag{6}$$

where e is the specific internal energy. The overall pressure is defined as the sum of the hydrodynamic (p) and the magnetic pressure,

$$P_G = p + \frac{1}{2} \frac{B^2}{\mu_0} \ . \tag{7}$$

The magnetic pressure is a stress acting normal to magnetic flux lines, similar to the hydrodynamic pressure in a stream line. It's also worth noting the last term on the r.h.s. of Eq. (2) is known as the hoop stress and acts along the magnetic flux lines, similar to the viscous tension (Moreau, 1990). Both terms originate from the replacement of the Lorentz force, $\mathbf{J} \times \mathbf{B}$, by the Maxwell stress tensor in Eqs. (2) and (3),

$$\mathbf{J} \times \mathbf{B} = \nabla \cdot \left(\frac{\mathbf{B}\mathbf{B}}{\mu_0} - \frac{B^2}{2\mu_0} \mathbf{I} \right) \ , \tag{8}$$

where $\mathbf{J}$ is the current density vector.

Equations (1-3) are differential equations for statements of conservation of mass, momentum and energy, respectively. Equation (4) is known as the induction equation and Eq. (5) is the divergence-free condition of the magnetic field.

2.2 Ideal and non-ideal MHD

Equation (4) describes the interaction between $\mathbf{B}$ and $\mathbf{U}$ and the propagation of the magnetic field, obtained by substituting Ohm's law in the Lorentz force. The propagation of $\mathbf{B}$ is dictated by two mechanisms. The first is the magnetic field convection, described by the first term on the r.h.s. of Eq. (4), and represents the change in the magnetic field due to the net balance resulting from the fluid particles entering and leaving an infinitesimal volume. The second mechanism, described by the the last term on the r.h.s. of Eq. (4), represents the diffusion transport of the magnetic field from regions with high electric current to low, responsible for smoothing the current density (Moreau, 1990). The ratio between the terms representing convective and diffusive transport give rise to the definition of the magnetic Reynolds number (Re_B),

$$Re_B \equiv \mu_0 \sigma L U \ , \tag{9}$$

where L is a characteristic length scale. For $Re_B \ll 1$, the convective term can be neglected. For $Re_B \approx 1$, the electromagnetic forces are ruled by the flowfield, so the convective and dissipative terms must be maintained in Eq. (4). In cases for which $Re_B \gg 1$, the diffusive term can be neglected. However, the equations will be strongly coupled and cannot be treated independently (Xisto *et al.*, 2010). This assumption leads to the ideal MHD equations, applied specially in the study of astrophysical phenomena, where $Re_B \to \infty$ and all hydrodynamic and magnetic dissipation effects are neglected (Boyd and Sanderson, 2003). Hence, in this limit, Eqs. (3) and (4) can be rewritten as,

$$\frac{\partial \rho E}{\partial t} + \nabla \cdot (\rho E \mathbf{U}) = -\nabla \cdot (P_G \mathbf{U}) + \frac{1}{\mu_0} \nabla \cdot [\mathbf{B} (\mathbf{B} \cdot \mathbf{U})] \ , \tag{10}$$

$$\frac{\partial \mathbf{B}}{\partial t} + \nabla \cdot (\mathbf{U}\mathbf{B} - \mathbf{B}\mathbf{U}) = 0 \ . \tag{11}$$

The proposed solver aims to solve both the ideal and non-ideal MHD set of equations.

2.3 Divergence free condition

Gauss's law for magnetism (Eq. 5) is as a constraint to ensure the conservative characteristic of the magnetic field. This is a central issue in numerical MHD, that if not treated correctly, can lead to numerical instability (Tricco and Price, 2012). In order to address this issue, the hyperbolic-parabolic cleaning approach described by Tricco and Price (2012), based on the one proposed by Dedner *et al.* (2002), is described briefly.

The method introduces a new potential variable ψ into Eq. (4),

$$\frac{\partial \mathbf{B}}{\partial t} + \nabla \cdot (\mathbf{UB} - \mathbf{BU}) - \frac{1}{\mu_0 \sigma} \nabla^2 \mathbf{B} + \nabla \psi = 0 \ . \tag{12}$$

Tricco and Price (2012) derived an equation for ψ using the energy associated to this field, in order to construct a formulation of hyperbolic divergence cleaning that is guaranteed to be stable. The resulting equation for ψ is,

$$\frac{\partial \psi}{\partial t} = -{c_h}^2 (\nabla \cdot \mathbf{B}) - \frac{{c_h}^2}{{c_d}^2} \psi - \frac{1}{2} \psi \nabla \cdot \mathbf{U} \ , \tag{13}$$

where c_h is the speed at which the error is convected and c_d acts as a dissipation coefficient. The idea is to spread the divergence error like a wave (with speed c_h) over a large area, enabling the parabolic term ($({c_h}^2/{c_d}^2)\psi$) to diffuse it more effectively, reducing it to zero (Tricco and Price, 2012). The c_h and c_d coefficients are given by,

$$c_h = \frac{\text{CFL}}{\Delta t \max(\frac{1}{d})} \ , \tag{14}$$

$$c_d = \sqrt{-\Delta t \frac{{c_h}^2}{\ln(C_r)}} \ , \tag{15}$$

where Δt is the time step and d is cell size, CFL is the Courant–Friedrichs–Lewy number and $0 < C_r < 1$. In this work $C_r = 0.9$ was used as in Mayigué and Groll (2016).

3. NUMERICAL METHOD

The application implemented is a modification of the algorithm *rhoCentralFoam* proposed by Greenshields *et al.* (2009), which makes use of the central scheme of Kurganov and Tadmor (2000) and the central-upwind scheme of Kurganov *et al.* (2001), while following an approach similar to the one used by Mayigué and Groll (2016), but taking into account dissipation effects and making use of a stable magnetic field divergence cleaning method.

As stated earlier, the algorithm was implemented in OpenFOAM, using the FVM to divide the spatial domain into a finite number of volumes. Each cell is assigned as an owner cell (P) and a neighbour cell (N). The face area vector $\mathbf{S}_f$ is a vector normal to the faces, pointing out of the cell P with magnitude equal to the area of the face. Figure 1 illustrates the FVM discretization. The vectors $\mathbf{d}$ and $\mathbf{d}_{fN}$ are the distance of the cell P to cell N and the distance of the cell face center to the centroid of the neighbour cell, respectively. The semi-discretization begins with the integration over a cell

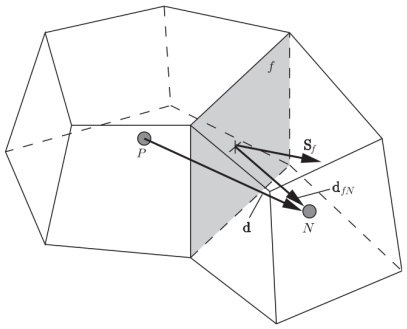

Figure 1: Finite volume discretization (Greenshields *et al.*, 2009).

volume V of the governing equations. Divergence and gradient terms are then converted into integrals over the cell face S using Gauss' theorem and linearized as follows,

$$\int_V \nabla \cdot (\mathbf{UW}) \, dV = \int_S (\mathbf{UW}) \cdot \mathbf{dS} \approx \sum_f \mathbf{U}_{f\pm} \mathbf{W}_{f\pm} \cdot \mathbf{S}_{f\pm} = \sum_f \phi_{f\pm} \mathbf{W}_{f\pm} \ , \tag{16}$$

here $\sum_f$ is a summation over cell faces, $\mathbf{W}$ is a vector of the conserved variables $(\rho, \rho\mathbf{U}, \rho E, \mathbf{B})$ and $\phi_{f,\pm} = \mathbf{U}_{f,\pm} \cdot \mathbf{S}_{f,\pm}$ is the volumetric flux through face f. The subindex f represents the variable interpolated onto the cell face and $\pm$ is the interpolation direction, $f-$ coincides with $-\mathbf{S}_f$ direction and $f+$ coincides with $+\mathbf{S}_f$.

The linear interpolation of $\mathbf{W}_f$ makes use of the weighting coefficient $w_f = |\mathbf{S}_f \cdot \mathbf{d}_{fN}|/|\mathbf{S}_f \cdot \mathbf{d}|$ as shown below (Greenshields *et al.*, 2009),

$$\mathbf{W}_f = w_f \mathbf{W}_P + (1 - w_f)\mathbf{W}_N \ . \tag{17}$$

This face interpolation needs to be stabilized based on transport that can occur in any direction. For that purpose, the KT (Kurganov and Tadmor, 2000) and the KNP (Kurganov *et al.*, 2001) methods are used as in Greenshields *et al.* (2009).

In these methods the interpolation is split into two directions corresponding to flow outward and inward of the face owner cell (denoted as $f+$ and $f-$, respectively) and the discretization of Eq. (16) is written as in Mayigué and Groll (2016),

$$\begin{aligned}\sum_f \phi_{f\pm}\mathbf{W}_{f\pm} = \sum_f \big[&\alpha\left(\phi_{f+}\mathbf{W}_{f+} + \kappa_{f+}\right) + (1-\alpha)\left(\phi_{f-}\mathbf{W}_{f-} + \kappa_{f-}\right) \\ &+\omega_f(\mathbf{W}_{f-} - \mathbf{W}_{f+}) + \frac{1}{2}(\Phi_{f-} - \Phi_{f+})\big] \ ,\end{aligned} \tag{18}$$

where the first two terms on the r.h.s. of Eq. (18) are flux evaluations in the $f+$ and $f-$ direction, respectively, and κ_f are terms related to the magnetic coupling into the conservation equations. The third term is only required in cases where the convection term is a part of a substantive derivative, i.e., Eqs. (2) and (3). It is an additional diffusion term using a volumetric flux ω_f based on the maximum speed of propagation of any discontinuity that may exist at the face (Greenshields *et al.*, 2009). The fourth term is employed by Mayigué and Groll (2016) for the treatment of the magnetic stress tensor and for the coupling of the potential variable ψ and the induction equation.

The variables $\mathbf{W}_{f\pm}$, $\kappa_{f\pm}$ and $\Phi_{f\pm}$ will assume different values according to the equation being solved (mass, momentum and energy conservation as well as the induction equation),

$$\mathbf{W}_f = \left(\rho,\ \rho\mathbf{U},\ \rho E + P_G,\ \mathbf{B}\right),\ \kappa_f = \left(0,\ \mathbf{S}_f P_G,\ -\frac{b_f}{\mu_0}(\mathbf{U}\cdot\mathbf{B}),\ -b_f\mathbf{U}\right),\ \Phi_f = \left(0,\ -\frac{\mathbf{B}b_f}{\mu_0},\ 0,\ \mathbf{S}_f\psi\right) \tag{19}$$

with $b_f = \frac{1}{2}(B_{f-} + B_{f+})$ and $B_{f\pm} = \mathbf{B}_{f\pm} \cdot \mathbf{S}_{f\pm}$.

The evaluation of the weighting factor α and the diffusive volumetric flux ω_f is related to the scheme used. For the KT method (central scheme), the contribution of the $f+$ and $f-$ are weighted equally, while the KNP method calculates α based on the one-sided local speeds of propagation (central upwind). Their values are defined as,

$$\alpha = \begin{cases} 1/2 & \text{for the KT method} \\ \Psi_{f+}/\left(\Psi_{f+} + \Psi_{f-}\right) & \text{for the KNP method} \end{cases} \tag{20}$$

$$\omega_f = \begin{cases} \alpha \max(\Psi_{f+},\ \Psi_{f-}) & \text{for the KT method} \\ \alpha(1-\alpha)(\Psi_{f+} + \Psi_{f-}) & \text{for the KNP method.} \end{cases} \tag{21}$$

Above, $\Psi_{f\pm}$ are volumetric fluxes associated with the speed of propagation and given by,

$$\Psi_{f+} = \max(c_f|\mathbf{S}_f| + \phi_{f+},\ c_f|\mathbf{S}_f| + \phi_{f-},\ 0) \ , \tag{22}$$

$$\Psi_{f-} = \min(c_f|\mathbf{S}_f| - \phi_{f+},\ c_f|\mathbf{S}_f| - \phi_{f-},\ 0) \ , \tag{23}$$

where $c_f = \min(c_+, c_-)$ is the propagation velocity, determined using the appropriate characteristic speed. In this work, following Mayigué and Groll (2016), the fast magnetosonic speed was employed, which is written as,

$$c_\pm = \left(\frac{1}{2}\left[{a^2}_\pm + {v^2}_{A,\pm} + \sqrt{\left({a^2}_\pm + {v^2}_{A,\pm}\right)^2 - 4{a^2}_\pm {v^2}_{A,\pm}\cos\theta^2}\right]\right)^{\frac{1}{2}} \ , \tag{24}$$

where θ is the angle between $\mathbf{B}$ and the $\mathbf{S}_f$ vectors, $a_\pm = \sqrt{\gamma RT}$ and $v_{A,\pm} = B/\sqrt{\mu_0\rho}$ are the the outward and inward states for the speed of sound and the Alfvén speed, respectively. The Alfvén speed refers to the velocity at which Alfvén waves propagate through a plasma or a magnetized medium.

Thus far, the discretization process has been shown only for the ideal MHD equations. To incorporate the effects of the non-ideal MHD, a conditional step is introduced: if the equations being solved are the non-ideal, the discretized

dissipative terms are included in the composition of the flux of the conservation of energy,

$$\underbrace{\sum_f \phi_{f\pm}(\rho E + P_G)_{f\pm}}_{\text{ideal MHD}} + \underbrace{\alpha\left[\frac{1}{{\mu_0}^2\sigma}(\mathbf{B}\cdot\nabla\mathbf{B})_{f+}\cdot\mathbf{S}_f\right] + (1-\alpha)\left[\frac{1}{{\mu_0}^2\sigma}(\mathbf{B}\cdot\nabla\mathbf{B})_{f-}\cdot\mathbf{S}_f\right] - \frac{1}{2{\mu_0}^2\sigma}\left(\nabla B^2\right)_f\cdot\mathbf{S}_f}_{\text{non-ideal MHD}} . \tag{25}$$

It is worth noting that for the energy conservation $\mathbf{W}_{f\pm}$ represents $(\rho E + P_G)_{f\pm}$.

Momentum and heat diffusion are treated with the same approach presented in Greenshields *et al.* (2009), where sequential operator splitting is applied in order to introduce the diffusive term as an implicit correction to the original inviscid equation.

Equation (13) for the potential variable ψ is solved semi-implicitly, where all terms are evaluated implicitly with the exception of the first term on the r.h.s., which is computed explicitly. Its discretized form is written as ${c_h}^2(\nabla\cdot\mathbf{B}) \approx {c_h}^2 b_f$. A sub-cycling routine was implemented in order to obtain a better estimate for ψ. For this, the fluid time step is divided in N-steps according to a user defined value.

The solution process occurs through the steps enumerated below.

1. ρ, $\rho\mathbf{U}$, e, $\mathbf{B}$, ψ and k are interpolated to cell faces, in order to obtain $\rho_{f\pm}$, $(\rho\mathbf{U})_{f\pm}$, $e_{f\pm}$, $\mathbf{B}_{f\pm}$, $\psi_{f\pm}$ and $k_{f\pm}$. Here $k = \rho/p$ is the compressibility.

2. $\mathbf{U}_{f\pm} = \frac{(\rho\mathbf{U})_{f\pm}}{\rho_{f\pm}}$, $\phi_{f\pm} = \mathbf{U}_{f\pm}\cdot\mathbf{S}_f$, $p_{f\pm} = \frac{\rho_{f\pm}}{k_{f\pm}}$, $P_{G,f\pm} = p_{f\pm} + \frac{{B_{f\pm}}^2}{2\mu_0}$ and $c_f = \min(c_+, c_-)$ are calculated, where $c_\pm$ is given by Eq. (24).

3. Governing equations are discretized and assembled using Eqs. (17 -23). For non-ideal MHD, the dissipative contributions in Eq. (25) are added to the energy conservation equation.

4. Conservation of mass, Eq. (1), is solved for ρ explicitly.

5. Conservation of momentum, Eq. (2), is solved for $\rho\mathbf{U}$. $\mathbf{U}$ is updated using $\mathbf{U} = (\rho\mathbf{U})/\rho$. For viscous flow, a diffusive velocity correction is solved implicitly for $\mathbf{U}$ (Greenshields *et al.*, 2009),

$$\frac{\partial(\rho\mathbf{U})}{\partial t} - \nabla\cdot(\mu\nabla\mathbf{U}) - \nabla\cdot\mathbf{T}_{exp} = 0 \tag{26}$$

   where μ is the dynamic effective viscosity and $\mathbf{T}_{exp} = \mu[(\nabla\mathbf{U})^T - \frac{2}{3}\text{tr}(\nabla\mathbf{U})\mathbf{I}]$ is the stress tensor containing inter-component coupling and is computed explicitly. Then $\rho\mathbf{U}$ is updated using the new value for $\mathbf{U}$.

6. Conservation of energy is solved for ρE and e is updated using Eq. (6). Diffusion is accounted by solving a diffusive energy correction equation, given by(Greenshields *et al.*, 2009),

$$\frac{\partial(\rho e)}{\partial t} - \nabla\cdot(\Gamma\nabla e) = 0 \ , \tag{27}$$

   where Γ is the effective diffusivity coefficient. Then ρE is updated with the new value of e and $\mathbf{U}$.

7. The induction equation (Eq. 12) is solved for non-ideal MHD cases, while for ideal MHD the second term on the r.h.s. is dropped.

8. Finally, Eq. (13) is solved in a sub-cycling routine.

4. RESULTS

Implementation and preliminary verification of the new solver, *mhdCentralFoam*, was done in OpenFOAM-v2212. The solver verification was performed by the simulation of two benchmark problems with either analytical solution or well documented solutions from established sources. These problems also have purely hydrodynamic solutions, allowing us to assess if the hydrodynamics are recovered if the magnetic field is set to zero.

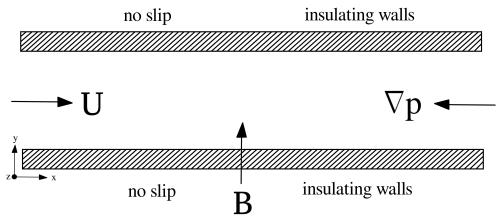

Figure 2: Hartmann flow problem visualization.

4.1 Hartmann flow

The flow consists of an electrically conducting fluid between parallel insulating plates with an applied transverse magnetic field, as depicted in Figure 2. The analytical solution for the velocity and magnetic field profiles are (Weller *et al.*, 1998),

$$\frac{U_x}{U_0} = \frac{\cosh(Ha) - \cosh\left(Ha\frac{y}{h}\right)}{\cosh(Ha) - 1} \ , \tag{28}$$

$$\frac{B}{U_0\mu_0\sqrt{\sigma\mu}} = -\frac{\frac{y}{h}\sinh(Ha) - \sinh\left(Ha\frac{y}{h}\right)}{\cosh(Ha) - 1} \ , \tag{29}$$

where h is the distance between the plates, U_0 is the velocity at the center of the domain, μ is the dynamic molecular viscosity and Ha is the Hartmann number, defined as the ratio between electromagnetic and viscous forces,

$$Ha = BL\sqrt{\frac{\sigma}{\mu}} \ . \tag{30}$$

For $\mathbf{B} = 0$ this case is equivalent to the Poiseuille flow with a parabolic velocity profile,

$$\frac{U_x}{U_0} = 1 - \left(\frac{y}{h}\right)^2 \ . \tag{31}$$

A rectangular two dimensional computational domain is considered, with length $l = 20$ m and height $h = 2$ m uniformly divided into 100 cells in x direction and 80 in y direction. The following boundary conditions are used: total pressure and temperature are imposed at inlet in order to assure that the Mach number (Ma) is equal to 0.01; at the outlet the pressure gradient is fixed. For upper and lower walls, the no slip condition is imposed and they are also considered electrically isolated with fixed magnetic field in the y direction. Three cases where analysed: purely hydrodynamic, i.e. $Ha = 0$, and two MHD cases with $Ha = 1$ and $Ha = 20$. Values used for the transport properties are: $\mu = 1$ kg/ms, $\mu_0 = 1$ H/m and $\sigma = 1$ $(\Omega\text{m})^{-1}$.

Figure 3 shows results for the purely hydrodynamic case. The solution computed by *mhdCentralFoam* agrees with the analytical solution. The results for the velocity and magnetic field profile in the MHD cases are presented in Fig. 4. Although the solver was able to capture the damping effect and the Hartmann layer, results show some deviation from the analytical solution, owing to the compressible nature of the solver. A small, albeit finite Mach number has to be defined in order to avoid numerical instabilities.

4.2 Brio-Wu shock tube

In order to test the solver for ideal MHD, the Brio-Wu shock tube was simulated (Brio and Wu, 1988). The MHD shock tube problem is a variation of the hydrodynamic shock tube problem of Sod (1978) and one of the best numerical examples for testing the ability of an MHD code to accurately describe the shocks, rarefaction, contact discontinuities and compound waves.

A rectangular one dimensional computational domain is simulated, with length $l = 2$ m ($-1 < x < 1$) divided in 1000 cells uniformly distributed in the x direction. Initial conditions are the same used by Brio and Wu (1988) and are shown in Fig. 5. Furthermore, the ratio of specific heats is $\gamma = 1.4$ for the purely hydrodynamic case (Sod's shock tube) and $\gamma = 2$ for the MHD case. In the purely hydrodynamic case results obtained are compared with those produced by *rhoCentralFoam* and the exact solution. As shown in Fig. 6, the solution obtained by *mhdCentralFoam* gives the exact same values produced by *rhoCentralFoam*. Both agree reasonably well with the exact solution, demonstrating the ability to capture discontinuities and rarefaction in the flow.

The MHD results are shown in Fig. 7 and compared with values from the Athena MHD code (Stone and Gardiner, 2008). It is clear that the solver implemented is able to capture all the phenomena involved with reasonable accuracy: the fast rarefaction and compound wave to the left and the contact discontinuity, slow shock and a second fast rarefaction

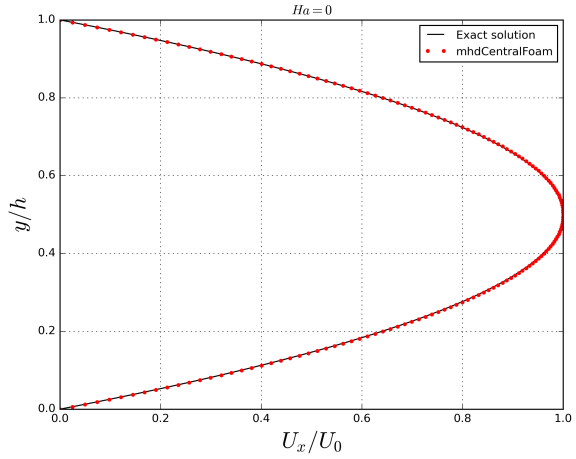

Figure 3: Comparison of the results for the hydrodynamic case ($Ha = 0$) with the exact solution.

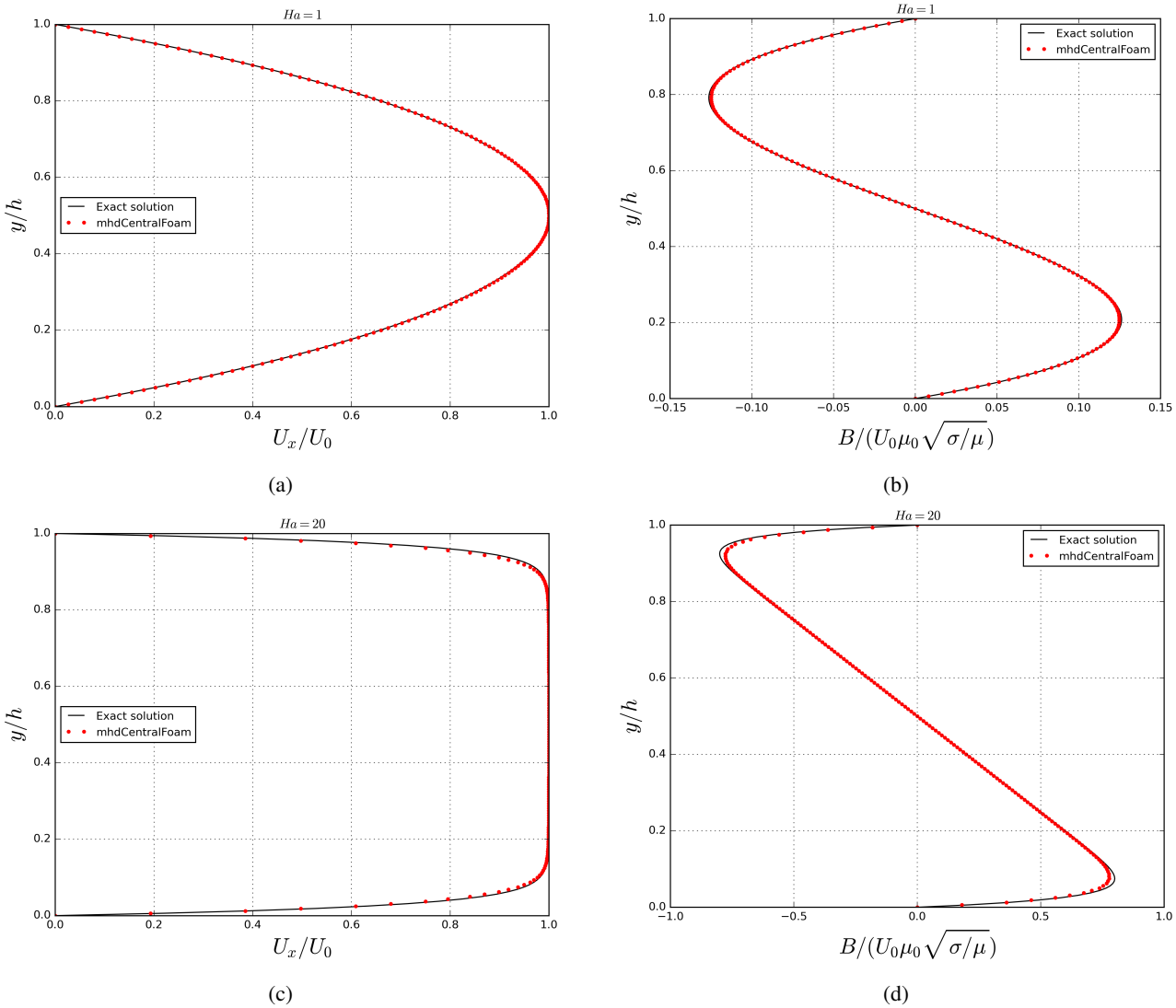

Figure 4: Results of the Hartmann flow for: (a) the velocity and (b) magnetic field profile at $Ha = 1$; (c) velocity and (d) magnetic field profile at $Ha = 20$.

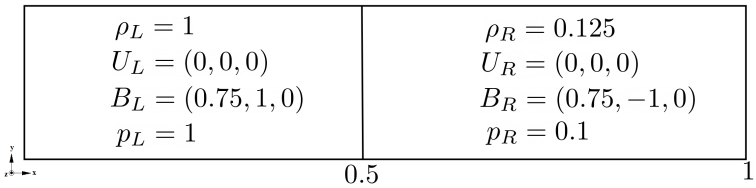

Figure 5: Geometry and initial conditions of the Brio-Wu shock tube. All values are in SI units.

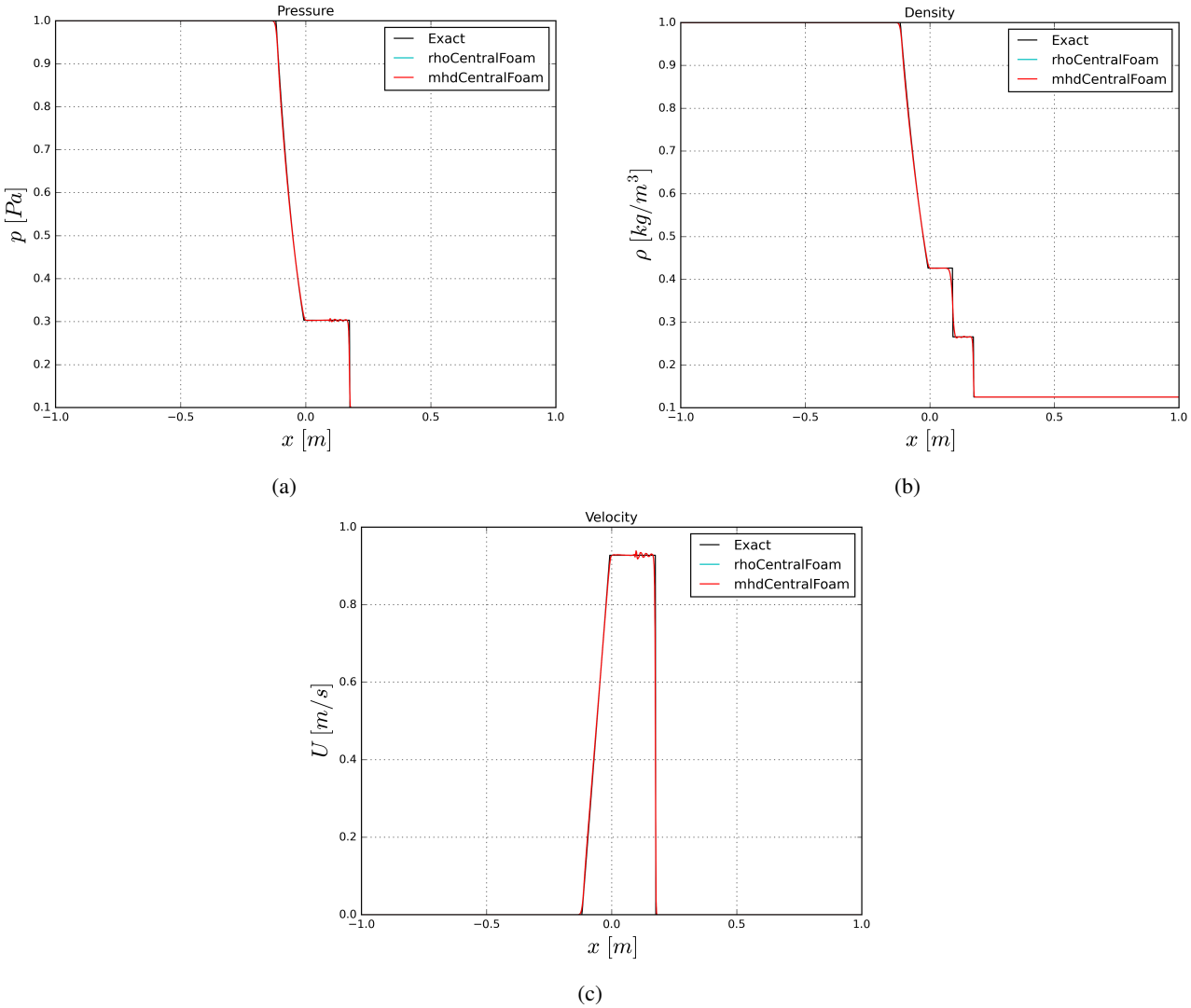

Figure 6: Comparison of the Sod's shock tube results, at $t = 0.1$ s for: (a) pressure p, (b) density ρ and (c) velocity magnitude U.

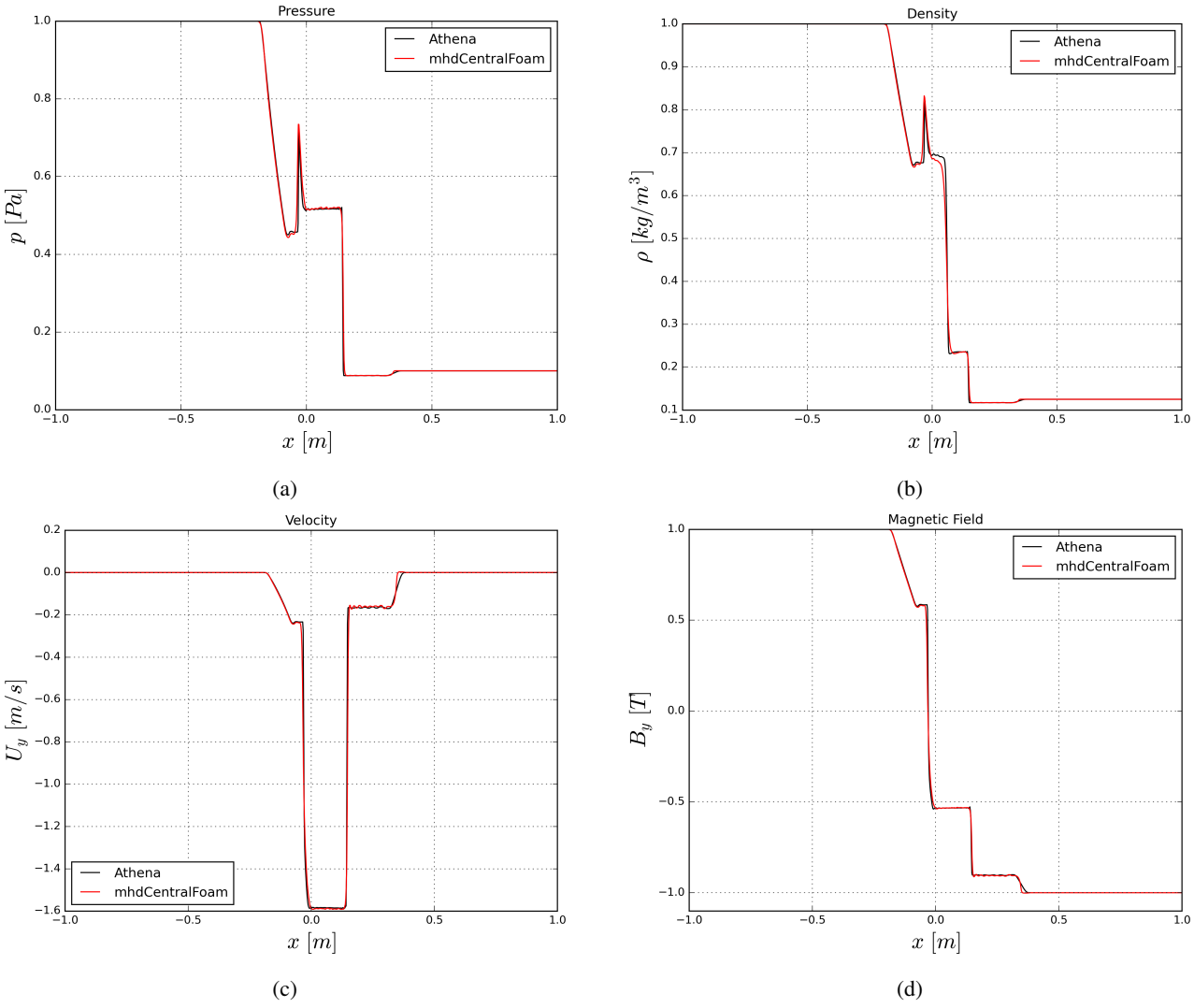

Figure 7: Results for the Brio and Wu shock tube, at $t = 0.1\ s$ for: (a) pressure p, (b) density ρ, (c) velocity component in the y direction U_y and (d) magnetic field component in the y direction B_y.

wave to the right. As in the purely hydrodynamic case, oscillations are present in the contact region. However, this is not related to any of the modifications implemented in the new solver. In fact, this behavior is also present in the solutions produced by *rhoCentralFoam* and is noted by Greenshields *et al.* (2009), indicating that such oscillations are related to the numerical method itself and not to the current implementation.

5. CONCLUSIONS

This work presents the first steps in the development of a compressible MHD solver that aims to simulate fluids in different regimes: ideal and non-ideal MHD for subsonic, transonic and supersonic flows. With the goal of evaluating and verifying the solver, results for two test cases are presented and compared with either analytical or well documented numerical solution available in the literature.

For the Hartmann flow the solver demonstrates ability to capture the physical phenomena, the damping effect due to transverse magnetic field and narrowing of the Hartmann layer. Solution inaccuracies are due to the compressible nature of our solver, albeit low Ma, whereas the Hartmann flow analytical solution is for incompressible flow.

Results for the Brio and Wu shock tube, demonstrate the new solvers ability to deal with compressible ideal MHD flows, and to accurately capture all physical phenomena such as contact discontinuity, compound waves and rarefaction. Oscillations present at the contact region are related to the numerical method and require further investigation.

Further work will be done to ensure the solenoidal nature of the the B-field and reduce unphysical oscillations at the contact discontinuity. The solver and pre-configured test cases can be downloaded at `https://codigos.ufsc.br/juan.salazar/mhdcentralfoam.git`

6. REFERENCES

Boyd, T.J.M. and Sanderson, J.J., 2003. *The Physics of Plasma*. Cambridge University Press, Cambridge.

Brio, M. and Wu, C.C., 1988. "An upwind differencing scheme for the equations of ideal magnetohydrodynamics". *Journal of Computational Physics*, Vol. 75, pp. 400–422.

Chen, G., Xiong, Q., Morris, P.J., Paterson, E.G., Sergeev, A. and Wang, Y.C., 2014. "Openfoam for computational fluid dynamics". *Notices of the AMS*, Vol. 61, pp. 354–363.

Davidson, P.A., 2001. *An introduction to magnetohydrodynamics*. Cambridge University Press, Cambridge.

Dedner, A., Kemm, F., Kröner, D., Munz, C.D., Schnitzer, T. and Wesenberg, M., 2002. "Hyperbolic divergence cleaning for the mhd equations". *Journal of Computational Physics*, Vol. 175, pp. 645–673.

Greenshields, C.J., Weller, H.G., Gasparini, L. and Reese, J.M., 2009. "Implementation of semi-discrete, non-staggered central schemes in a colocated, polyhedral, finite volume framework, for high-speed viscous flows". *International Journal for Numerical Methods in Fluids*, Vol. 63, pp. 1–21.

Kurganov, A., Noelle, S. and Petrova, G., 2001. "Semidiscrete central-upwind schemes for hyperbolic conservation laws and hamilton-jacobi equations". *SIAM Journal on Scientific Computing*, Vol. 23, pp. 707–740.

Kurganov, A. and Tadmor, E., 2000. "New high-resolution central schemes for nonlinear conservation laws and convection–diffusion equations". *Journal of Computational Physics*, Vol. 160, pp. 241–2842.

Mayigué, C.C. and Groll, R., 2016. "A density based method with semi-discrete central-upwind schemes for ideal magnetohydrodynamics". *Archive of Applied Mechanics*, Vol. 62, pp. 667–683.

Moreau, R., 1990. *Magnetohydrodynamics*. Fluid Mechanics and its Applications. Springer Science+Business Media Dordrecht.

Sod, M., 1978. "A survey of several finite difference methods for systems of nonlinear hyperbolic conservation laws". *Journal of Computational Physics*, Vol. 27, pp. 1–31.

Stone, J.M. and Gardiner, T.A., 2008. "Athena: a new code for astrophysical mhd". *The Astrophysical Journal Supplement Series*, Vol. 178, pp. 137–177.

Tang, T. and Wang, Y., 2015. "On the ideal compressible magnetohydrodynamic equations". *Journal of Mathematical Analysis and Applications*, Vol. 430, pp. 1–19.

Tricco, T.S. and Price, D.J., 2012. "Constrained hyperbolic divergence cleaning for smoothed particle magnetohydrodynamics". *Journal of Computational Physics*, Vol. 231, pp. 7214–7236.

Weller, H.G., Tabor, G., Jasak, H. and Fureby, C., 1998. "A tensorial approach to computational continuum mechanics using object-oriented techniques". *Computers in Physics*, Vol. 12, pp. 620–631.

Xisto, C.M., Páscoa, J.C., Oliveira, P.J. and Nicolini, D.A., 2010. "Implementation of a 3d compressible mhd solver able to model transonic flows". In *V European Conference on Computational Fluid Dynamics ECCOMAS CFD 2010*. ECCOMAS - The European Community on Computational Methods in Applied Sciences, Lisbon, Portugal.

7. RESPONSIBILITY NOTICE

The authors are solely responsible for the printed material included in this paper.